ROLE OF THERMAL CONDUCTION IN THE ACCELERATION OF THE SOLAR WIND

Stanislaw Olbert
Center for Space Research and Department of Physics
Massachusetts Institute of Technology
Cambridge, Massachusetts 02139

ABSTRACT

The thermal and suprathermal processes involving solar wind electrons are discussed from a theoretical point of view. A model for the electron distribution function, f_e, based on the solutions of the Boltzmann equation in Krook's approximation is outlined: the angular and energy dependences of f_e for various distances from the sun between the coronal base and the earth are presented with the express purpose of obtaining the radial profile of the heat flux generated by the suprathermals. The calculations take into account the effects of the morphology of the interplanetary magnetic field, the electrostatic polarization potential and coulomb scattering, but assume that, as far as the suprathermals are concerned, the effects of wave-particle interactions are negligible. This surmised knowledge of the heat flux allows us to solve the basic fluid-dynamical equations for the solar wind plasma as a whole along any given magnetic field line. The results, although containing a variety of idealizing assumptions, are in surprisingly good agreement with observations. In particular, the predicted density and temperature profiles for positive ions exhibit the characteristics of recent measurements, both in the corona (above the coronal holes) and between 0.3 and 1 A.U. (the Helios region). It is concluded that the suprathermal electrons play an important role in the formation and the dynamics of the solar wind.

1. Introduction

The discovery of Coronal Holes confirmed a belief of long standing that the stream structure of the solar wind in the steady state is closely related to the morphology of the magnetic field lines in the corona. The open field lines in the regions above the Coronal Holes serve as a nozzle for the coronal plasma to flow into the far regions of the Heliosphere. The high-velocity streams observed by various spacecraft can be thought of as originating in the central portion of a Coronal Hole above the coronal base (say, between 1.03 $r_\odot$ and 1.50 $r_\odot$). Enough information is now available to surmise empirical radial profiles of the macroscopic parameters of such high-velocity streams. Figures 1, 2, and 3 show, respectively, typical radial dependences of the interplanetary magnetic field, the plasma density and the electron and proton temperatures. Several features of these profiles merit special emphasis: 1) the radial component of the magnetic field, $\vec{B}$, between 1.03 $r_\odot$ and 2 $r_\odot$ decreases much more rapidly than the $(1/r^2)$ field of the spherical model; 2) the density above Coronal Holes is substantially lower than the average and exhibits a much steeper gradient; 3) the temperature of the core electrons can be approximated roughly by an empirical polytropic relation: $T_c \propto n^\beta$ where $\beta \simeq .185$ and n is the density; 4) the proton

temperature displays a strong correlation with the wind velocity (in particular, the high-velocity streams are characterized by high temperature protons). This last point deserves further elaboration: Helios data show that the proton temperature, T_p, in a high-velocity stream grows rapidly as one approaches the Sun and reaches about one million degrees at 0.3 A.U. This type of radial dependence of T_p precludes any possibility of a polytropic relation between T_p and n.

The above sketched features of the solar wind beg for a physical explanation. As a first step in this direction, we have initiated a "feasibility" study of a model that emphasizes the role of the suprathermal electrons in the heat conduction along any given field line. We have attempted to adhere to first principles and the empirical facts as much as possible, and purposely ignored the possible importance of any other ad hoc driving mechanism. In other words, we have attempted to answer the following question: Do the suprathermal electrons generate enough heat flux to drive a high-velocity solar wind? The following is the preliminary report of our findings to date.

2. Basic Equations for the Field-aligned Solar Wind Flow

We confine our discussion to a steady field-aligned flow along a radial tube of force emanating from the central portion of a given Coronal Hole and concern ourselves only with the inner region of the solar cavity (from 1.03 $r_\odot$ to 1 A.U.). This allows us to ignore the effects of the rotation of the Sun and the curvature of the field lines. Furthermore, we assume that the r-dependence of B is known on empirical grounds. Finally, except for the appearance of a new term for the heat flux, we take the basic MHD equations as valid. Using standard notation, (B for the magnitude of the magnetic field, V for the wind speed, ρ for the mass density, P for the thermal pressure of electrons and positive ions combined, and $\vec{q}$ for the heat flux vector) we have for the plasma as a whole:

$$\rho V = \alpha B \tag{1}$$

$$\rho V \frac{dV}{dr} = - \frac{dP}{dr} - \rho G \frac{M_\odot}{r^2} \tag{2}$$

$$\frac{3}{2} \rho^{5/3} V \frac{d}{dr} \left(\frac{P}{\rho^{5/3}} \right) = - \operatorname{div} \vec{q} \tag{3}$$

where α is a streamline constant. Eq. (1) follows from conservation of mass (div($\rho\vec{V}$)=0) and magnetic flux (div $\vec{B}$=0). Equations (2) and (3) express

150

conservation of momentum and energy, respectively. Note that, since $\vec{q}$ is field aligned, one can replace div $\vec{q}$ by $\vec{B} \cdot \nabla$ $(\vec{q} \cdot \vec{B}/B^2)$ or, for our geometry,

$$\text{div } \vec{q} = \frac{dW}{dr} \rho V \tag{4}$$

where

$$W = \frac{q}{\alpha B} = \frac{q}{\rho V} \tag{5}$$

If the function W is assumed to be a known function of the radial distance, r, or alternatively, of any of the dependent dynamical variables ρ, V, P, equations (1), (2) and (3) represent a closed system of equations for three unknowns: ρ, V and P. Two of these unknowns can be eliminated immediately. First, Equations, (2) and (3) yield the integral:

$$\frac{1}{2} V^2 + \frac{5P}{2\rho} - \frac{GM_\odot}{r} + W = \frac{1}{2} U^2 \tag{6}$$

where U is a streamline constant representing the asymptotic value of the wind speed. Equation (6) allows us to eliminate P in terms of remaining variables. Secondly, Equation (1) allows the elimination of, say, V in favor of ρ. We obtain after some algebra, the following first-order differential equation for ρ:

$$\frac{r}{\rho} \frac{d\rho}{dr} = \frac{H(\rho, r)}{L(\rho, r)} \tag{7}$$

where

$$H = \frac{3r dB}{B \ dr} \left(\frac{\alpha B}{\rho}\right)^2 + \frac{3GM_\odot}{r} \tag{8}$$

$$L = 4\left(\frac{\alpha B}{\rho}\right)^2 + 2W + 2\rho \frac{dW}{d\rho} - \frac{2GM_\odot}{r} - U^2 \tag{9}$$

In Section 4, we shall explain the procedures which we used to construct an explicit form of W as a function of ρ. For the present, we need only the result. Figure 4 shows the (dimensionless) quantity W/U^2 plotted versus electron density n_e; it has been computed under the assumption that $\alpha^2 = 2.4 \times 10^{-23}$ g/cm^3, $U^e = 700$ km/sec and that B of Figure 1 may be approximated by the empirical formula:

$$B = 2.2 \left(\frac{r_s}{r}\right)^2 \sqrt{1+47 \left(\frac{r_s}{r}\right)^6} \quad \text{(gauss)} \tag{10}$$

where $r_s \equiv 1.03 \, r_\odot$.

For the purpose of numerical integration of Equation (7), we found it convenient to represent W in Figure 4 by an analytical formula:

$$\ln\left(\frac{W}{W_0}\right) = 0.0514 \ln\left(\frac{\rho}{\rho_0}\right) + 2.87 \, \text{erf}\left(0.2 \ln \frac{\rho}{\rho_0}\right) \tag{11}$$

where $\rho_0 \simeq 10^{-22}$ g/cm^3 and $W_0 \simeq 10^4$ (km/sec)^2

3. Numerical Calculations of (ρ, V, P) profiles

Detailed analytical study near the critical point of Equation (7) (i.e., the radial distance r_c at which H=L=0) has shown that Equation (7) allows a two-branch solution through r_c: one for the accretion and one for the outflow. The topology of the solution in the neighborhood of the critical point is analogous to that of the polytropic Parker model. Figure 5 shows the density profile corresponding to the outflow with U=700 km/sec. A comparison of Figure 2 data referring to the high-velocity streams (lower segments of the n_e curves) reveals an excellent agreement with the curve of Figure 5. Once the density profile is obtained, it is a simple matter to compute the remaining profiles for V and P. Figure 6 shows the wind-speed profile based on Equations (1) and (10) and Figure 7 shows the quantity:

$$T_{eff} = \frac{P}{2kn_e} \tag{12}$$

Since $P \simeq k(n_e T_c + n_p T_p + n_\alpha T_\alpha)$ (n_α and T_α indicate the number density and the temperature of the α-particles, respectively) - T_{eff} may be interpreted as the "effective" temperature of a high-velocity stream. A comparison of the T_{eff} -curve with the combined data for T_c, T_p and $T_\alpha \simeq 4T_p$ in the explored region of the heliosphere (r > 0.3 A.U.) shows a surprisingly good agreement both in slope and the levels of the ion temperatures. The agreement is improved further when a (relatively minor) correction for the presence of the Alfvén-wave pressure is made in the expression for P. Of course, the unexpected result of our calculations lies in the unexplored region (2 $r_\odot$ < r < 0.3 A.U.): T_{eff} exhibits a rise with a maximum of 2.5x10^6 °K at 9 $r_\odot$. Since the core-electron temperature in our model decreases monotonically with r (see next section) and thus at 9 $r_\odot$ is substantially lower than 2.5x10^6 °K, one is forced to conclude that the model requires surprisingly high proton and α-particle temperatures in the outer

152

regions of the corona. We must stress that if one accepts the form of the heat flux used in the calculations, this conclusion is forced upon us by nothing else but the basic laws of conservation of mass, momentum and energy. Since our form of the heat flux predicts correct density profiles of the high-velocity streams, we find the conclusion inescapable.

4. Heat Flux Calculations

We now outline briefly the method and the steps that we have taken to arrive at the result shown in Figure 4. Space limitation does not allow us to go into detail but only to mention that one can develop a variety of cogent arguments demonstrating that the conventional theory for heat conduction in collision dominated plasma (e.g., Spitzer's theory) is not applicable to any portion of the solar corona. The traditional Fourier law $(q_{\shortparallel} = -K \nabla_{\shortparallel} T)$ breaks down right at the base of the corona where $T \simeq 10^6$ °K and $n_e \simeq 10^8$ cm^{-3}. This is so in spite of the fact that the coulomb mean free path (mfp) of thermal electrons, $\bar{\lambda}_c$, at the base is still very small compared to the solar radius $(\bar{\lambda}_c \simeq 10^{-3} r_\odot)$. The main reasons for it are: a) the mfp grows rapidly with the electron energy (a suprathermal electron of 7kT has a mfp 50 times larger than $\bar{\lambda}_c$); b) the steep density gradient above Coronal Holes leads to a short scale height H (H $\simeq$ 0.1 $r_\odot$); c) small H leads to a rapid development of skewness in the distribution function of suprathermals; and d) the forward skewness of suprathermals is fostered by the paucity of collisions and the open line morphology of the rapidly decreasing magnetic field. For these reasons, any perturbation method relying on the smallness of the Knudsen number $(\bar{\lambda}_c/H)$ will lead to erroneous results concerning the physical characteristics of the heat flux. The reader is invited to read more on this in the paper presented by J. Scudder during these proceedings.

There seems to emerge from these types of considerations a clear cut possibility: the suprathermals may carry enough heat to drive the solar wind. To check this in a quantitative manner we saw no way out but to rely on the first principles of the plasma kinetic theory, i.e., to evaluate first the electron distribution function, f_e, at various points along some given tube of force and then by direct numerical integration compute the heat flux at these points. Since the solution of the Boltzmann equation for f_e in its more rigorous form (say, in the Fokker-Planck approximation) is prohibitively difficult, we have opted for the Krook's approximation which, although not as accurate as the Fokker-Planck approximation, is on physical grounds far superior to any perturbation method (such as that of Chapman and Enskog).

First, let us list the simplifications that can be made in the general Boltzmann equation. We are interested in the distribution function, f_e, of transthermal and suprathermal electrons. For these electrons, the proper plasma frame and the inertial heliocentric frame of reference practically coincide. The gravitational effects are negligible. Moreover, f_e is gyrotropic, i.e., in the steady state, f_e is a function of only three variables: radial distance r, the speed v and pitch angle θ. With these stipulations, f_e (r,v,θ) obeys the following equation:

$$v \cos\theta \frac{\partial f_e}{\partial r} - \frac{eE_{\shortparallel}}{m_e} \cos\theta \frac{\partial f_e}{\partial v}$$

$$+ \left(\frac{eE_{\shortparallel}}{m_e} + \frac{v^2}{2B}\frac{\partial B}{\partial r}\right) \frac{\sin\theta}{v} \frac{\partial f_e}{\partial \theta} = - \frac{f_e - f_M}{\tau} \tag{13}$$

where $E_{\shortparallel}$ is the component of the electric field parallel to $\vec{B}$ and is related to "interplanetary polarization potential", ϕ, by $E_{\shortparallel} = -d\phi/dr$; τ is the mean coulomb collision time for momentum transfer and is given by

$$\frac{1}{\tau(r,v)} = \xi \frac{4\pi e^4 n_e \ln\Lambda}{m_e^2 v^3} \tag{14}$$

In our case the numerical factor $\ln\Lambda \simeq 25$ and ξ is of order of unity. For the "source function" f_M, which coincides approximately with that of the distribution of the core electrons, we adopt a maxwellian form

$$f_M(r,v) \simeq \frac{n_e}{\pi^{3/2} w_c^3} e^{-v^2/w_c^2} \tag{15}$$

where w_c is the thermal speed related to the temperature, T_c, of the core electrons by $m_e w_c^2 = 2kT_c$. Note that the number density, n_e, and w_c are functions of r. Other forms for f_M, compatible with observations of thermal and subthermal electrons, may be chosen to improve the description of the electron transport. The reader will find more on this in the aforementioned report by J. Scudder. Since the brunt of the dynamical processes shaping the evolution of the solar wind takes place in the coronal region, we are primarily concerned about the adequacy of Equation (15) in that region. Since in the limit of τ being very small f_e should approach a maxwellian form, Equation (15) ought to represent a reasonable first step in an iteration process to which Equation (13) could be subjected. Note that in the limit of a very large τ (collisionless plasma) Equation (13) has a well known general solution

$$f_e = \psi(E,\mu) \tag{16}$$

where ψ is any appropriately chosen function of the two constants of motion:

$$E = \frac{1}{2} m_e v^2 - e\phi; \quad \mu = \frac{m_e v^2 \sin^2\theta}{2B} \tag{17}$$

Not much is known about f_e for finite τ's. But it turns out that Equation (13) can be integrated formally for any given form of f_M and τ by methods of characteristics. If one confines oneself to the particle trajectories in the forward direction $(0 \leq \theta \leq 90°)$ one finds:

$$f_e(r,v,\theta) = f_M(r,v) - \int_{r_0}^{r} \frac{df_M(r',v')}{dr'} e^{-p(r,r';v,\theta)} dr' \tag{18}$$

where

$$v' = \sqrt{v^2 + \frac{2e}{m_e}(\phi(r') - \phi(r))} \tag{19}$$

and

$$p(r,r';v,\theta) = \int_{r'}^{r} \frac{dr''}{\tau(r'',v'')v''\cos\theta''} \tag{20}$$

In Equation (20) v'' is given by Equation (19) upon replacing r' by r''

and

$$\cos\theta'' = \sqrt{1 - \sin^2\theta \frac{B(r'')v^2}{B(r)v''^2}} \tag{21}$$

Note that, for a fixed r, v and θ, Equation (21) imposes a lower limit r_m on r' given implicitly by the equation:

$$\frac{v_m^2}{B(r_m)} = \sin^2\theta \frac{v^2}{B(r)} \tag{22}$$

where v_m is given by Equation (19) upon replacing r' by r_m; r_m is the point where $\theta'' = 90°$, i.e., the mirror point of the trajectory. This implies that care must be taken while evaluating Equation (18) that the inequality chain:

$$r_0 \leq r_m \leq r' \leq r'' \leq r \tag{23}$$

155

be not broken; r_0 identifies the boundary of the onset of the outward heat flow. The precise value of r_0 cannot be ascertained, but it ought to fall somewhere between 1.03 $r_\odot$ and 1.30 $r_\odot$; fortunately, f_e for $r > 2\ r_\odot$ is not sensitive to r_0. The explicit numerical evaluation of Equation (18) requires the knowledge of n_e, T_c, ϕ and B as functions of r. We made the following choices:

$$n_e(r) = n_1 \exp[13.25 - 5.50\ \ln \frac{r}{r_s} + 3.50 \sqrt{(\ln \frac{r}{r_s} - 0.82)^2 + .79}] \qquad (24)$$

$$T_c(r) = T_1 (\frac{n_e}{n_1})^\beta \qquad (25)$$

$$\phi(r) = \omega k T_c; (\omega = 1 + \frac{1}{\beta}) \qquad (26)$$

B is assumed to be given by Equation (10)

and $\qquad\qquad \beta = 0.185,\ T_1 = 8\times10^4\ °K,\ n_1 = 2\ cm^3.$

In constructing formulas (24) and (25) we were guided by the observational data referring to the high-velocity streams. Equation (24) reproduces well the Coronal Hole and the high speed profiles of Figure 2. Equation (25) agrees with the dashed curve in Figure 3 and the empirical findings of Sittler and Scudder; its validity in the solar corona must remain at the present moment an open question although the numerical values it offers in the inner corona are not in contradiction with the observational estimates. Equation (26) is primarily based on theoretical considerations involving the generalized Ohm's law; for our purposes, it is in a sufficiently good agreement with the findings of other authors; but again, its validity in the inner corona must remain an open question.

The entire subject matter of finding self-consistent functional relations between n_e,T_c and ϕ from the first principles is still unresolved. It is a subject of current investigations by Dr. Scudder and myself.

"Armed" with the empirical formulas (24) through (26), we are in a position to evaluate f_e as a function of v and θ, for various values of r. Since the computer costs involving this project have proven to be very high, we had to confine ourselves to only six values of r (r/r_s = 1, 2, 4.7, 16, 63 and 208). Figures 8, 9, 10 and 11 show the forward portions of the contours of constant f_e plotted in the velocity space for r/r_s=2,4.7,16 and

156

and 63. Note that the coordinates are $v_\parallel$ and $v_\perp$ measured in terms of the local thermal speed, i.e., the horizontal coordinate is $v \cos\theta/w_c$ and the vertical coordinate is $v \sin\theta/w_c$. The ratio of the values of f_e of two neighboring contours is $\sqrt{10}$; the outermost (lowest value) contour corresponds to $f_e = 8\times10^{-31}$ $(sec/cm^2)^3$. As one proceeds outward from the Sun one witnesses a gradual evolution of a highly skewed, forward "strahl", very much like the strahl observed onboard Helios spacecraft. There are various other features in the distribution that are of potential value from the plasma-theoretical point of view; e.g., the development of a col in the transthermal region of the velocity space. Such cols are sources of various plasma waves which in turn affect the thermal electrons. Clearly, the results shown here open up a new area of future investigations.

We have not computed the backward portions of the distribution function ($90° < \theta < 180°$) for the simple reason that we believe that f_e cannot develop any significant backward "strahl" and, for the purposes of the heat flux calculations, may be approximated by a maxwellian form for all speeds.

The knowledge of f_e allows us to compute the heat flux q at various values of r. We have

$$q(r) = \pi m_e \int\int v^5 \cos\theta \ f_e(r,v,\theta) \ \sin\theta \ d\theta \ dv \qquad (27)$$

Because of the complexity of f_e as a function of v and θ, the double integration required to obtain q is enormously expensive and we had to confine ourselves to the six r-values quoted above. Thus, the entire effort leaves us with only six numbers which must serve us as "beacons" for the construction of the curve shown in Figure 4. Needless to say, we had to take some liberties to perform the necessary interpolation leading to the results shown in Figure 4.

Finally, we should like to comment why we have chosen to represent the function $W=q/(\alpha B)$ as a function of density rather than as a function of distance. Firstly, purely on practical grounds, it is more economical to evaluate f_e when one replaces the integration variable r' in Equation (18) by $n_e(r')$ or $T_e(r')$ via Equation (24) or (25). Secondly, the dependence of W on r is primarily predicated by its dependence on n_e. Thus, on physical grounds, it is more instructive to know W as a function of n_e rather than as a function of the arclength along a specific field line. This does not mean to imply that W may be looked upon as a unique function n_e for all field lines. On the contrary, our calculations show that q is quite sensitive to the behavior of the magnetic field. Since the possibility for relating B to n_e by some theoretical "law" is quite remote, we must treat B and n_e as separate entities and thus regard W as a function of n_e and B.

5. Summary

Our preliminary calculations show that the heat flux generated by the suprathermal electrons plays an important role in the dynamics of the solar

wind. In fact, there is a possibility that it might account entirely for the salient features of steady, pure high-velocity streams. Of course, more work is required to resolve the issue, but we believe that the initial results presented here invite such work as worthwhile.

FIGURE CAPTIONS

Figure 1: Typical radial profile of the interplanetary magnetic field, $\vec{B}$. Except for the shaded area near the Sun, the curves are based on Parker's spiral model and are in agreement with observations averaged over fluctuations.

Figure 2: Typical radial profiles of the electron number density, n_e, in the solar wind. The curves were constructed from a variety of observational sources. The two lower segments labeled "density above polar Coronal Hole" and "fast streams" are characteristic of the central portion of a high-velocity stream.

Figure 3: Typical radial profiles of proton and electron temperatures in the solar wind. The solid curves represent the scalar proton temperature, $T_p = (1/3)(2T_\perp + T_\parallel)$, for three adjacent intervals of the wind speed, I, II and III. The dashed curve refers to the core electron temperature, T_c; the dot-dashed curve, labeled T_H, represents $7T_c$ and is meant to indicate the domain of the suprathermals. Except for the tentative markings near the Sun, the plots are a "smoothed out" version of the Helios and Voyager data.

Figure 4: The heat conduction W, measured in terms U^2 and plotted versus electron number density, n_e; W is related to the heat flux q by: $W = q/(\rho V) = q/(\alpha B)$. See text for the definition of symbols and the theoretical considerations leading to this plot. (The arrow labeled C.P. indicates the position of the critical point).

Figure 5: Calculated radial profile of the electron number density, n_e. The curve represents the "critical" solution of Equation (7) (see text) and should be compared with the lower segments of the data of Figure 2.

Figure 6: Calculated radial profile of the wind speed, V. The curve is computed from $V = \alpha B/\rho$ using the result shown in Figure 5. The point labeled C.P. indicates the position of the critical point.

Figure 7:   Calculated radial profile of the "effective temperature" of a
            high-velocity stream (see text for the definition of T_{eff} and P).

Figure 8:   Contours of constant electron distribution function, f_e, plotted
            in the velocity space for $r = 2r_s$. The horizontal (vertical)
            coordinate represents the parallel (perpendicular) component of
            the electron velocity measured in terms of the local thermal
            speed, w_c. The ratio of two neighboring contours is $\sqrt{10}$; the
            outermost (lowest) contour represents $f_e = 8 \times 10^{-31}$ $(sec/cm^2)^3$.
            The figure implies gyrotropy and shows only the forward portion
            of f_e $(0° \leq \theta \leq 90°)$; $r_s = 1.03$ $r_\odot$.

Figures 9, 10 and 11:   Same as Figure 8 but referring, respectively, to
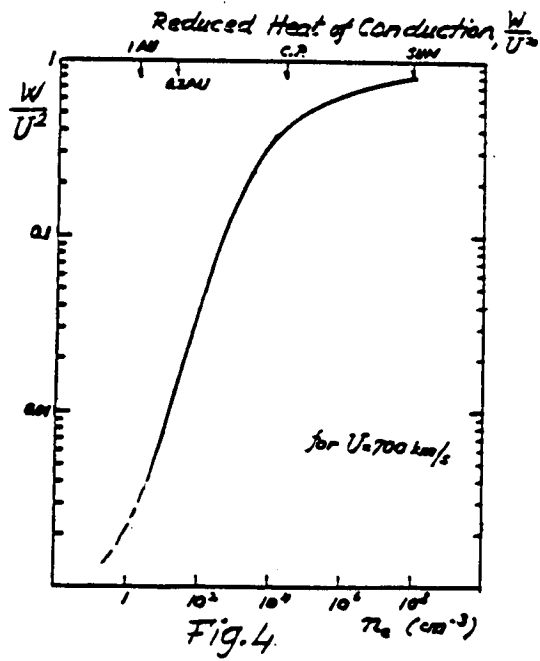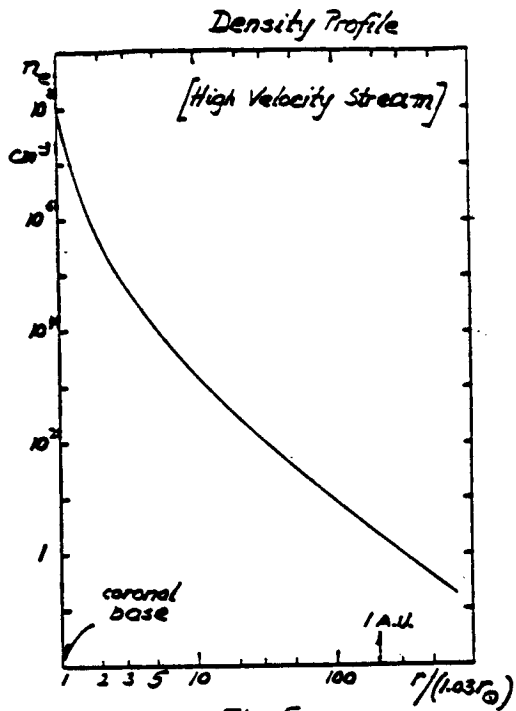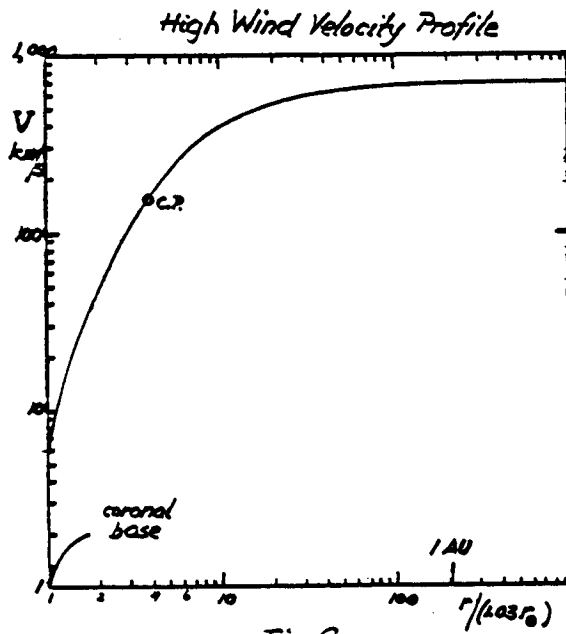 $r/r_s = 4.7$, 16 and 63.

Fig. 1

Fig. 2

Fig. 3

Fig. 4

Reduced Heat of Conduction, $\frac{W}{U^2}$

Density Profile

[High Velocity Stream]

n_e

cm^{-3}

coronal base

1 A.U.

$r/(1.03 r_\odot)$

Fig. 5

High Wind Velocity Profile

V
$\frac{km}{s}$

c.p.

coronal base

1 AU

$r/(1.03 r_\odot)$

Fig. 6

Effective Temperature Profile

[High Velocity Stream]

T

$T_{eff}^{calc.} = \frac{P}{2 k n_e}$

coronal base

1 AU

$r/(1.03 r_\odot)$

Fig. 7

$\frac{u_\perp}{u_c}$

$\bar{n} = 2 n_s$

$\frac{v_\parallel}{u_c}$

Fig. 8

161

$\tau = 4.7 \tau_s$

Fig. 9

$\tau = 16 \tau_s$

Fig. 10

$\tau = 63 \tau_s$

Fig. 11